

**Report on Data Pipeline Development  
for Grain Boundary Structures Classification**

**By**

**BINGXI LI**

**B.E. (Northwestern Polytechnical University) 2014**

**M.S. (University of California, Davis) 2016**

**REPORT**

**Submitted in partial satisfaction of the requirements for the degree of**

**MASTER OF SCIENCE**

**in**

**Computer Science**

**in the**

**OFFICE OF GRADUATE STUDIES**

**of the**

**UNIVERSITY OF CALIFORNIA**

**DAVIS**

**Approved:**

---

**Prof. Norman S. Matloff, Chair**

---

**Prof. Francois Gygi**

**Committee in Charge**

**2017**

---

Bingxi Li  
September 2017  
Computer Science

Report on Data Pipeline Development  
for Grain Boundary Structures Classification

**Abstract**

Grain Boundaries govern many properties of polycrystalline materials, including the vast majority of engineering materials. Evolutionary algorithm can be applied to predict the grain boundary structures in different systems. However, the recognition and classification of thousands of predicted structures is a very challenging work for eye detection in terms of efficiency and accuracy. A data pipeline is developed to accelerate the classification and recognition of grain boundary structures predicted by Evolutionary Algorithm. The data pipeline has three main components including feature engineering of grain boundary structures, density-based clustering analysis and parallel K-Means clustering analysis. With this data pipeline, we could automate the structure analysis and develop better structural and physical understanding of grain boundaries.

*September 29, 2017*

# List of Figures

1	A scheme of USPEX evolutionary prediction. . . . .	4
2	Structure model and evolutionary operations for prediction. . . . .	7
3	Two dimensional visualization of the algorithm. (A) Point distribution. Data points are ranked in order of decreasing density. (B) Decision graph for the data in (A). Different colors correspond to different clusters. [29] . . . . .	10
4	The heterogeneous architecture for OpenACC ( <a href="https://www.OpenACC.org/">https://www.OpenACC.org/</a> ). 13	
5	Representative structures from three popular kites family of GB structures [35]. . . . .	18
6	Split Kite Family. Split kites of five representative boundaries predicted by the evolutionary search and clustering analysis. These GB structures are viewed parallel to [001] tilt axis in left column and normal to it in right column. . . . .	19
7	Extended Kite family. Three representative Extended Kite phases are predicted by the evolutionary search at 0 K. The misorientation angles are indicated on the figure. For each misorientation GB structures as viewed parallel to the [001] tilt axis in left and normal to it in right. . . . .	20
8	Evolutionary search and clustering identify new ground states and multiple grain boundary phases. The search explores different atomic densities and finds low-energy grain boundary configurations (green circles) ignored by the conventional methodology. With same tilt angle $\theta$ atomic fractions and energies of each grain boundary at 0 K are colored by blue triangles for Kite family , red diamonds for Split Kite family and orange squares for Extended Kite family. . . . .	21
9	Eye detection of $\sum 5(210)$ in the 2-dimensional space of excess stress and volume, where the direction of excess stress $F_x$ is parallel to tilt axis. The orange dots correspond to distorted structures while the green, blue and purple are for Filled Kite(FK), Normal Kite(K or NK) and Split Kite(SK) respectively. . . . .	22
10	Decision graph of $\sum 5(210)$ when the criterion distance is equal to (a)1DC, (b)1.56DC, (c)2DC. . . . .	23

11	The clustering of GB structures in $\Sigma 5(210)$ system on different feature maps (a) Excess $Q_4$ vs Excess Stress $F_X$ , (b) Excess Stress $F_X$ vs Atomic Fraction, (c) Excess Stress $F_X$ vs Excess volume, (d) Excess $Q_6$ vs Excess $Q_4$ , (e) Excess $Q_6$ vs Atomic Fraction, (f) Excess $Q_6$ vs Excess Volume, (g) Excess $Q_{12}$ vs Excess $Q_4$ , (h) Excess Volume vs Excess Energy, (i) Excess $Q_{12}$ vs Excess Volume. . . . .	24
12	The clustering of GB structures in $\Sigma 29(520)$ system on different feature maps (a) Excess $Q_4$ vs Excess Stress $F_X$ , (b) Excess Stress $F_X$ vs Atomic Fraction, (c) Excess Stress $F_X$ vs Excess volume, (d) Excess $Q_6$ vs Excess $Q_4$ , (e) Excess $Q_6$ vs Atomic Fraction, (f) Excess $Q_6$ vs Excess Volume, (g) Excess $Q_{12}$ vs Excess $Q_4$ , (h) Excess Volume vs Excess Energy, (i) Excess $Q_{12}$ vs Excess Volume. . . . .	25
13	The clustering of GB structures in $\Sigma 5(310)$ system on different feature maps (a) Excess $Q_4$ vs Excess Stress $F_X$ , (b) Excess Stress $F_X$ vs Atomic Fraction, (c) Excess Stress $F_X$ vs Excess volume, (d) Excess $Q_6$ vs Excess $Q_4$ , (e) Excess $Q_6$ vs Atomic Fraction, (f) Excess $Q_6$ vs Excess Volume, (g) Excess $Q_{12}$ vs Excess $Q_4$ , (h) Excess Volume vs Excess Energy, (i) Excess $Q_{12}$ vs Excess Volume. . . . .	26
14	The GB structures in $\Sigma 5(310)$ system (a) Kite Family (NK or K), (b) NKdeform2SK , (c) Split Kite family (SK). . . . .	27
15	The GB structures in $\Sigma 5(310)$ system (a) Kite Family (NK or K), (b) NKdeform2SK , (c) Split Kite family (SK). . . . .	28
16	The GB structures in $\Sigma 37(610)$ system Kite Family (NK or K) in the left , NKmixSK, NKdeform2SK and NKBigKitedeform2SK in the middle while Split Kite family (SK) in the right. . . . .	29

# Contents

<b>1 Introduction</b>	<b>1</b>
1.1 Grain Boundary Structures . . . . .	1
1.2 Evolutionary Search . . . . .	2
1.3 Motivations of Data Pipeline Development . . . . .	4
<b>2 Components of Data Pipeline</b>	<b>6</b>
2.1 Feature Engineering of Grain Boundary Structures . . . . .	6
2.1.1 Evolutionary Predicted Structures . . . . .	6
2.1.2 Construction of Feature Space . . . . .	7
2.2 Clustering Analysis . . . . .	8
2.2.1 Density Based Clustering Analysis . . . . .	8
2.2.2 Parallel K-means Clustering Functionality . . . . .	10
<b>3 Implementation</b>	<b>12</b>
3.1 GB structure calculations at 0 K . . . . .	12
3.2 Density Clustering . . . . .	13
3.3 Parallel Implementation of K-Means Algorithm . . . . .	13
3.3.1 3 Steps to Accelerate with OpenACC . . . . .	14
3.3.2 Parallel Directives . . . . .	14
3.3.3 Optimization Techniques . . . . .	17
<b>4 Results</b>	<b>17</b>
4.1 Grain boundary energy as a function of angle and atomic density .	17
4.2 Clustering results for the grain boundary . . . . .	18
4.3 Clustering of Grain Boundaries with Low Tilt Angle . . . . .	22
<b>5 Discussions</b>	<b>28</b>
<b>6 Acknowledgments</b>	<b>30</b>
<b>7 Running Demo</b>	<b>30</b>

# 1 Introduction

## 1.1 Grain Boundary Structures

Cleaner energy conversion and more efficient energy utilization generated increasing demand in the development of advanced metallic alloys and ceramics that can safely perform under extreme conditions. The performance and properties of these structural and functional materials are greatly determined by the existence of internal interfaces called grain boundaries (GB) during materials synthesis and processing. Therefore it is significant to understand the grain boundary structures and their influence on materials properties.

In previous studies, interfacial structures existing in different states are called *complexions* [1, 2]. Complexion types are characterized by different amounts of impurity segregation. Different types of complexions including monolayer, bilayer, trilayer and thicker inter-granular films have been suggested [1]. Grain boundary complexions was firstly predicted and well studied by earlier theoretical researches with phase model for their roles in first-order and high order transition [3–5]. Experimental studies suggested a potential role of complexions transitions on abnormal grain growth in ceramics [1], activated sintering [6], and liquid metal embrittlement [7]. Recently, GB complexions has been also applied to lattice dislocations, revealing the existence of new states of GB called linear complexions. All of the above studies suggested the importance of GB in determining the behaviors and structural properties of materials [8, 9].

While the experimental investigation of the influence of grain boundary on materials properties is currently a highly active field [10–13], the atomic details of these grain boundary phases remain unclear. It is extremely difficult to have direct experimental observations of interface phase transitions at high temperature by HRTEM due to inherent limitations [14]. Although many HRTEM studies of grain boundaries in doped metallic and ceramic materials showed grain boundary structures are similar inter-granular films of different thickness [1, 2, 10, 15], these HRTEM images are of low resolution and cannot provide more detailed atomistic structure of these boundaries, which make the results and conclusions less convincing.

Atomistic simulations is promising to predict atomic structure of interfaces and study their thermodynamic and kinetic properties.  $\gamma$  surface method has been developed and well accepted as a common approach to build grain boundaries in atomistic simulations. It has been employed to study interfaces in a variety of materials for more than four decades. However an increasing number of recent studies suggested an alternative approaches of grain boundary construction and pointed out that  $\gamma$ -surface method is limited to predict true ground states.

For example, a recent investigation of two high angle boundaries  $\Sigma 5(210)[001]$  and  $\Sigma 5(310)[001]$  in Cu demonstrated the root cause of missing transformations is the inadequate simulation methodology with constant number of atoms and periodic boundary conditions. An alternative high-temperature anneals of these boundaries connected to open surfaces allowed the variation of atom numbers in grain boundary to achieve lower free energy states [16, 17]. The simulations revealed multiple new grain boundary phases of the boundaries are impacted by different atomic densities and demonstrated fully reversible first-order transitions induced by temperature, changes in chemical compositions and point defects. This ingenious modeling approach demonstrated phase behavior of two special high-angle boundaries that have been extensively investigated in the past still missed entire phenomenon which are overlooked by modeling with previous restrictive simulation methodology.

Recognizing the limitations of current modeling capabilities and the obstacle to observing grain boundary phase transitions, a robust computational tool is required to predict complex grain boundary structures.

## 1.2 Evolutionary Search

In recent years, there have been significant advances in predicting the structures from first-principles calculations. Among them, evolutionary algorithm has proved to be extremely powerful in different systems including bulk crystals [18], 2D crystals [19], surfaces [20], polymers [21] and clusters [22], etc. It is very promising to extend the method to predict grain boundary structures.

A few pioneering works have been reported in the literature [23–25]. However there are some limiting facts about these previous work. For instance, Chua et al

developed a genetic algorithm to study the non-stoichiometric grain boundaries of  $SrTiO_3$  [24]. It can only be applied for a system with fixed number of atoms and super-cell size. In my research, an evolutionary algorithm based software **Universal Structure Predictor: Evolutionary Xtallography (USPEX)** [18] is used. It enables the automated exploration of GB structures with variable number of atoms and cell sizes in higher dimensional space. Here is an outline steps and a scheme Fig 1 of USPEX prediction.

The 7 steps are:

1. Prepare adequate representations for the problem: a one-to-one correspondence between the point in the search space and a set of numbers.
2. Initiate the first generation, which consists of a set of points in the search space satisfying the constraints of the problem.
3. Determine the quality of each member of the population with the fitness function.
4. Select the “best” member of the population as the parents and apply the variation to create the new points (offspring).
5. Evaluate the new member of the new population.
6. Select the “best” member of offspring to form the new generation of the population.
7. Repeat step 4 to 6 until reaching the halting criteria.

It is well-known that the complexity exponentially increases with the growing dimensionality. Therefore to ensure efficient sampling, it is significant to balance between individual quality and population diversity. Naive random structure initialization or variation operation will only lead to disordered-like structures but with close energetics. To address this challenge, the implementation in USPEX utilizes coarse-grained modeling and defines the simplified representations when generating structures. Some key representations including symmetry, vibrational modes and degree of local order are used here.

With the powerful prediction tool based on evolutionary algorithms, we are able to predict structures of interfaces. In the iterations of Fig 1, USPEX generates



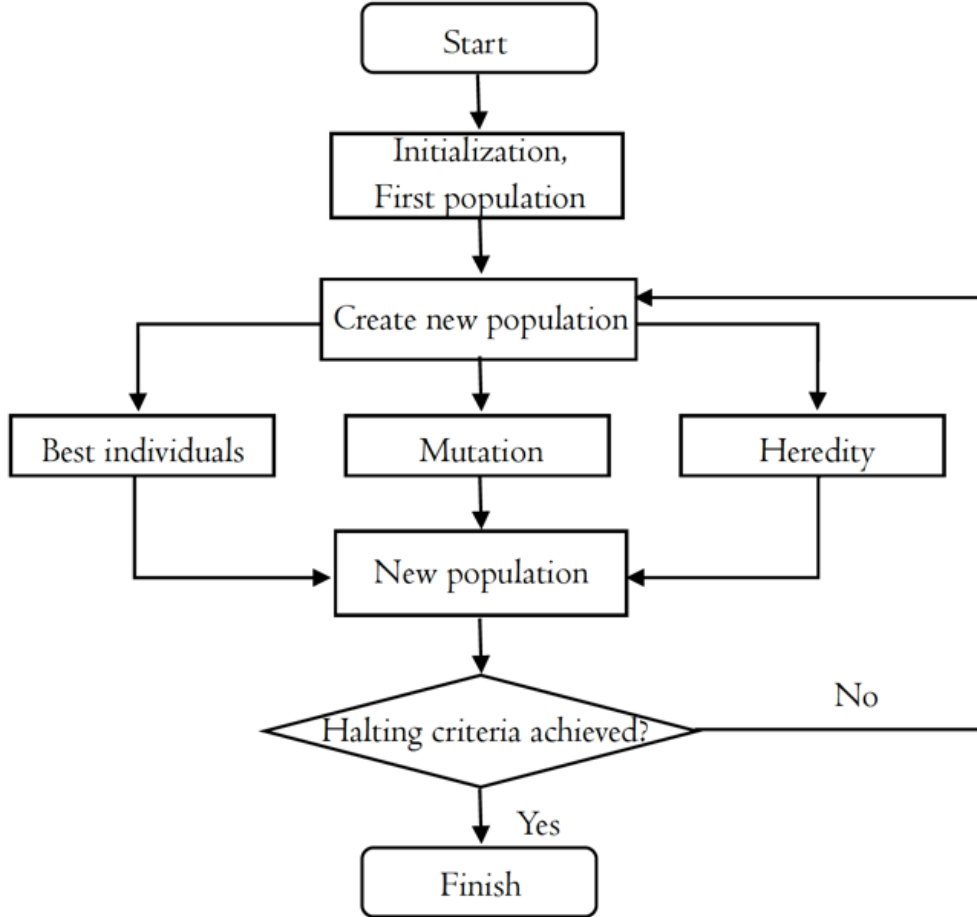


Figure 1: A scheme of USPEX evolutionary prediction.

a population of grain boundary structures and optimize them over several generations to predict configurations of low-energetics. During the evolutionary convergence process, complex and diverse structures with different atomic densities are sampled by operations of heredity and mutation which involve atomic rearrangements like addition and removal of atoms from the grain boundary core.

### 1.3 Motivations of Data Pipeline Development

In simulation, the evolutionary algorithm generates thousands of GB structures in every prediction run to Cu system with different tilting angle  $\theta$ , ranging from  $11.42^\circ$  to  $79.61^\circ$ . Here are challenges in analysis over such a large number of GB structures.

**Undefined Problems** Most of the GB structures are first time to observe and

very few studies can be referenced when classifying and understanding these GB structures. So there is no clear and complete definition of GB structures in Cu system with different tilting angles. Besides, most of these structures are disordered or mixed with different complexions. Some structures that exist in Cu system with certain angles miss in other system with different tilting angles. This makes the existence of GB structures inconsistent through a wide range of tilting angles. A convincing way to represent and describe GB structures is therefore necessary.

**Lacking of Robust Classification** It is quite time-consuming to classify over thousands of structures through eye detection. This process needs laboring work and detailed check and comparisons for multiple times, which greatly reduce the efficiency of GB discovery.

To solve the above challenges, solutions are proposed as follows:

**Mapping GB Structure in Lower Dimensional Space** It is clear that the GB structure is originally represented in  $3N$ -dimensional space, where  $N$  is the number of atoms in GB structures. Therefore a technique to reduce dimension is required. In my work, every GB structure is represented in a feature space composed by structural and mechanical properties including excessive free energy, excessive volume, stress tensors, Steihardt order parameters ( $Q_4, Q_6, Q_8, Q_{12}$ ). Through this feature engineering work, a problem in  $3N$ -dimensional space is then reduced into one in 8-dimensional feature space or properties space.

**Density Based Clustering Algorithm** The categorization of the GB structures is actually the learning of non-labeled data, which is equally a unsupervised learning problem. Clustering algorithm is very promising for this type of problem. However, conventional clustering algorithm like K-means clustering algorithm requires prior knowledge to select the value for K, which limits the power of this algorithm. A density based clustering algorithm proposed by Rodriguez, Alex and Laio, Alessandro can yield reasonable K value without any domain knowledge. All the data can be clustered with  $O(1)$  iterations, namely without self-consistent process.

To integrate the feature engineering and density based clustering algorithm, I

developed the data pipeline to automate the whole analysis. It has been proved to be very helpful and useful in the GB structures analysis.

## **2 Components of Data Pipeline**

In this section, I would like to introduce the ideas behind every component of the data pipeline.

### **2.1 Feature Engineering of Grain Boundary Structures**

Firstly, I will give a brief review of the grain boundary structure model and the evolutionary prediction.

#### **2.1.1 Evolutionary Predicted Structures**

In Fig 2 The GB model used for into three different regions, the region of upper grain (UG) and lower grain (LG), and grain boundary (GB). The evolutionary algorithm adopts concepts from evolutionary biology based on populations, selection, reproduction by heredity and mutation to optimize the individual with highest fitness. The code generates a population of grain boundary structures and improves them over several generations to predict low-energy configurations. During the evolution complex and diverse structures with different atomic densities are sampled by operations of heredity and mutation which involve atomic rearrangements as well as addition and removal of atoms from the grain boundary core.

The evolutionary algorithm adopts three operations populations, selection, reproduction by heredity and mutation to optimize the individual with highest fitness. The code generates a population of grain boundary structures and improves them over several generations to predict low-energy configurations. During the evolution complex and diverse structures with different atomic densities are sampled by operations of heredity and mutation which involve atomic rearrangements like addition and removal of atoms from the grain boundary core.

The Evolutionary Prediction finally output different configurations of grain boundary structures. And these structures are represented as set of atomic coordinates

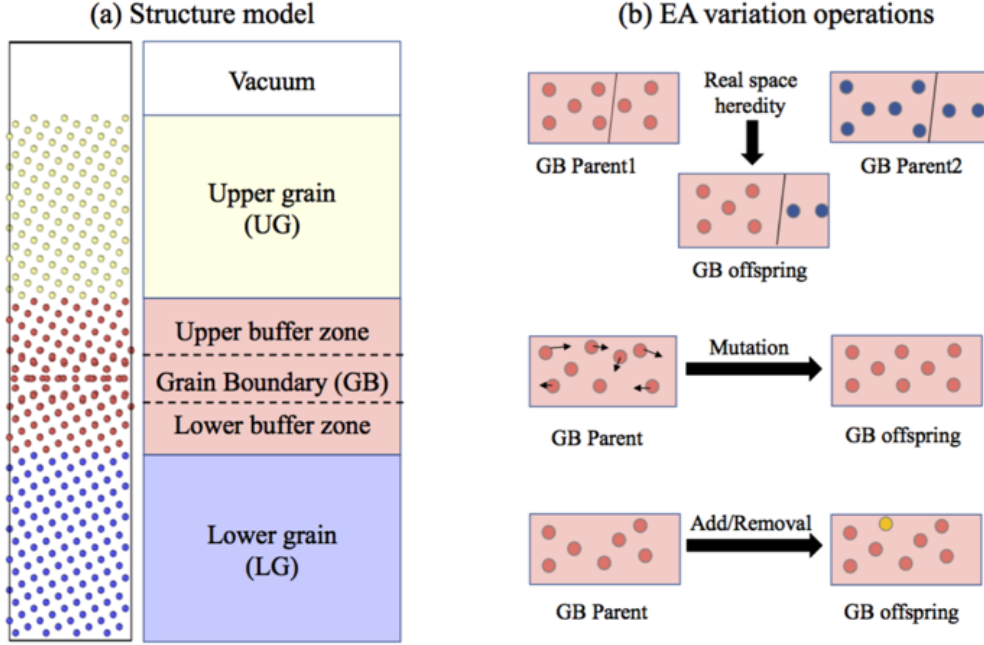


Figure 2: Structure model and evolutionary operations for prediction.

in 3-dimension Cartesian space. Thus, every structure is a data point in  $3N$ -dimensional space, where  $N$  is the number of atoms that configure the structure.

### 2.1.2 Construction of Feature Space

Eight excessive properties are calculated from the GB region and bulk region shown in Fig 2. The excessive properties are excessive free energy  $[\gamma]_N$ , atomic volume  $[V]_N$ , stress  $[\tau]_{11}$ , stress  $[\tau]_{22}$  and Steinhardt order parameter  $[Q_4]_N$ ,  $[Q_6]_N$ ,  $[Q_8]_N$ ,  $[Q_{12}]_N$  [26].

In a single component system, grain boundary free energy  $\gamma_{GB}$  is given with following equation.

$$\gamma A = E - TS - \sigma_{33}V = [E]_N - T[S]_N - \sigma_{33}[V]_N \quad (1)$$

where  $[Z]_X$  are grain boundary excess properties expressed with Cahn's determinants. According to the adsorptions equation [27], grain boundary free energy is also a function of temperature, stress and lateral strain.

$$d(\gamma A) = -[S]_N dT - [V]_N d\sigma_{33} + \tau_{ij}A de_{ij} \quad (2)$$

where  $i, j = 1, 2$ . At OK, the excess volume  $[V]_N$  and two components of grain boundary stress  $\tau_{11}$  and  $\tau_{22}$  per unit of grain boundary area can be computed as,

$$\begin{aligned} [V]_N &= \frac{1}{A} \left( V - V^{bulk} \frac{N}{N^{bulk}} \right) \\ \tau_{11} &= [\sigma_{11} V]_n = \frac{1}{A} \left( \sigma_{11} V - \sigma_{11}^{bulk} V^{bulk} \frac{N}{N^{bulk}} \right) \\ \tau_{22} &= [\sigma_{22} V]_n = \frac{1}{A} \left( \sigma_{22} V - \sigma_{22}^{bulk} V^{bulk} \frac{N}{N^{bulk}} \right) \end{aligned} \quad (3)$$

Notice that  $\frac{V^{bulk}}{N^{bulk}} = \Omega$  is a volume per atom in the bulk. In atomistic simulations volume occupied by each atom is calculated by LAMMPS with the Voronoi construction [28]. The product  $\sigma_{ij} V$  for each atom can also be calculated by LAMMS. In our calculations bulk stresses are zero within the numerical accuracy.

Besides the four features described above, excess amounts of Steinhardt order parameters of grain boundary is also used, including  $Q_4$ ,  $Q_6$ ,  $Q_8$  and  $Q_{12}$  [26]. These parameters per atom are calculated within LAMMPS [28]. The equation for this calculation is,

$$[Q]_N = \frac{1}{A} \left( Q - Q^{bulk} \frac{N}{N^{bulk}} \right) \quad (4)$$

where  $Q = \sum_{i=1}^N Q^i$  is the total amount of the order parameter per atom in a region enclosing the grain bulk and containing  $N$  atoms,  $\frac{Q^{bulk}}{N^{bulk}}$  is the value of this order parameter per atom in the bulk, where  $Q$  is one of the  $Q_4$ ,  $Q_6$ ,  $Q_8$  or  $Q_{12}$ .

The above excessive properties calculation takes the grain boundary structure in form of atomic coordinates as input. Therefore after the calculations to 8 excess properties for every structure, we finally map each structure in  $3N$ -dimensional space into a data point in 8-dimensional feature space.

## 2.2 Clustering Analysis

### 2.2.1 Density Based Clustering Analysis

With the above mapping techniques, GB structure can be represented as a vector  $f$  in the feature space, where

$$f = ([\gamma]_N, [V]_N, \tau_N^{11}, \tau_N^{22}, [Q_4]_N, [Q_6]_N, [Q_8]_N, [Q_{12}]_N) \quad (5)$$

The density based clustering algorithm [29] is actually a visualized methodology. It firstly remap the vector for data  $i$  in the feature space onto a two dimensional plot where the x, y axis are density  $\rho_i$  and  $\delta_i$ , which measures the minimum distance between the point  $i$  and any other point with higher density.

Therefore for each data point  $i$ , we need to compute two quantities: its local density  $\rho_i$  and its distance  $\delta_i$  from points of higher density. Both these quantities depend on the distances  $d_{ij}$  between data points, which are assumed to satisfy the triangular inequality. For the local density  $\rho_i$  of data point  $i$ , it is defined as the Euclidean distance between structure  $i, j$  in this abstract space.

$$d_{ij} = \|f^i - f^j\|_2 = \sqrt{\sum_{n=1}^8 (f_n^i - f_n^j)^2} \quad (6)$$

The local density  $\rho_i$  of data point  $i$  is defined as,

$$\rho_i = \sum_j \chi(d_{ij} - d_c) \quad (7)$$

where  $\chi(x) = 1$  if  $x < 0$  and  $\chi(x) = 0$  otherwise,  $d_c$  is a cutoff distance. It can be simply expressed as the number of points that are closer than  $d_c$  to point  $i$ . The algorithm is only robust with a good choice of  $d_c$ . And the choice of  $d_c$  can be well derived with following visualization way.

For the  $\delta_i$ , it is assigned with following equation,

$$\delta_i = \min_{j:\rho_j > \rho_i} (d_{ij}). \quad (8)$$

while for the point with highest density, we conventionally take  $\delta_i = \max_j (d_{ij})$ . Note that  $\delta_i$  is much larger than the typical nearest neighbor distance only for points that are local or global maxima in the density. Thus, cluster centers are recognized as points for which the value of  $\delta_i$  is anomalously large.

In Fig 3, the algorithm in two dimension is described with an example of 28 data points. Fig 3A contains 28 points. It can be seen that points 1 and 10 are the density maxima, which we identify as cluster centers. Fig 3 shows the points distribution on the plot of  $\rho$  and  $\delta$ . This representation is a decision graph. From

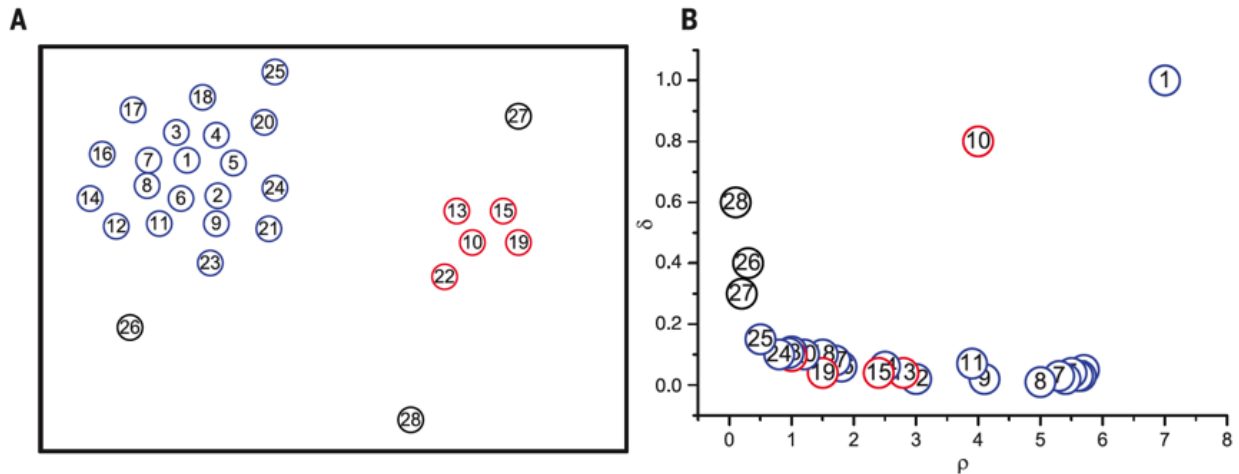


Figure 3: Two dimensional visualization of the algorithm. (A) Point distribution. Data points are ranked in order of decreasing density. (B) Decision graph for the data in (A). Different colors correspond to different clusters. [29]

the graph, we could see that the value  $\rho$  of points 9 and 10 is similar while their values of  $\delta$  is very different. Point 9 belongs to the cluster of centering around point 1, and several other points with a higher  $\rho$  are very close to it, whereas the nearest neighbor of higher density of point 10 belongs to another cluster. Hence, as anticipated, the only points of high  $\rho$  and relatively high  $\delta$  are the cluster centers. Points 26, 27, and 28 have a relatively high  $\delta$  but with a low  $\rho$ . This is because they are isolated. They can be regarded as clusters of a single point or outliers [29].

A great advantage of this algorithm is that after assigning the cluster centers, each remaining point is assigned to the same cluster as its nearest neighbor of higher density. Therefore, the decision graph can be computed within  $O(n^2)$  time complexity and  $O(n)$  space complexity, where  $n$  is the number of GB structures. The cluster assignment is performed in a constant step, in contrast with other clustering algorithms which usually need to optimize the objective function iteratively [30, 31].

### 2.2.2 Parallel K-means Clustering Functionality

K-means clustering is a popular method for cluster analysis in data mining. It aims to partition  $n$  observations into  $k$  clusters in which each observation belongs to the cluster with the nearest mean, serving as a prototype of the cluster. As a result of K-means clustering, the data space will be partitioned into Voronoi cells.

The most common algorithm uses an iterative refinement technique. The popular one is often referred as Lloyd’s algorithm. It starts with an initial set of  $k$  means  $m_1^{(1)}, \dots, m_k^{(1)}$ . Then the algorithm proceeds by alternating between two following steps [31]:

1. **Assignment step:** Assign each observation to the cluster whose mean has the least squared Euclidean distance. This mathematically means partitioning the observations according to the Voronoi diagram generated by the means.

$$S_i^{(t)} = \{x_p : \|x_p - m_i^{(t)}\|_2^2 \leq \|x_p - m_j^{(t)}\|_2^2 \forall j, 1 \leq j \leq k\} \quad (9)$$

2. **Update step:** Calculate the new means to be the centroids of the observations in the new clusters.

$$m_i^{(t+1)} = \frac{1}{|S_i^{(t)}|} \sum_{x_j \in S_i^{(t)}} x_j \quad (10)$$

The algorithm has converged when the assignments no longer change. However it does not guarantee that the optimum found using this algorithm.

### Motivations to Explore Parallelism in K-Means Algorithm

K-means algorithm is a very simple and powerful method for clustering analysis. However, finding the optimal solution to the k-means clustering problem for observations in  $d$  dimensions is a NP-hard problem [32]. There were a variety of heuristic algorithms such as Lloyd’s algorithm given above are generally used. The running complexity of Lloyd’s algorithm is  $O(nkdi)$  [33], where  $n$  is the number of entities represented as  $d$ -dimensional vectors to cluster and  $k$  the number of clusters,  $i$  being the number of iterations needed until convergence.

The number of iterations until convergence is only small, on data that have a cluster structure. Results can improve slightly after the first dozen iterations. Lloyd’s algorithm is therefore often considered to be of “linear” complexity in practice. But in worst case, it is superpolynomial [34]. Another thing that makes the case even worse is the large quantity of data. We are in a world of big data today. Most of clustering algorithms unavoidably face the challenges raised by massive data.



Through the above analysis, we see the rapid complexity growth of this algorithm when clustering over data at large scale. Therefore it will be very promising to explore the potential parallelism in current algorithm and accelerate it on powerful parallel platform.

### **Parallelism in K-Means Algorithm**

The parallelism is obvious in the assignment step. The serial version will take  $O(N^2)$  time complexity. However the distance computation have data independence to use, which means the assignment of data  $i$  can be done simultaneously with data  $j$ . To explore the data-level parallelism, some parallel computation model like CUDA C and OpenACC are very favorable. Compared to CUDA, OpenACC requires much less programming effort to parallelize serial code.

## **3 Implementation**

This section discusses some details of the data pipeline implementation.

### **3.1 GB structure calculations at 0 K**

Each grain boundary was generated from 3-5 independent evolutionary searches. Each search evolves up to fifty generations. The search explores different atomic densities ranging from 0 to 1 measured as a fraction of number of atoms found in one bulk atomic plane parallel to the grain boundary. A typical run explores the structures ranging from 500 to 5000 atoms for the entire model and 30 to 300 atoms for the GB region. The different grain boundary areas of each grain boundary are explored by replicating the smallest possible cross-section up to 25 times. LAMMPS code [28] was used to evaluate the energy of every generated configurations.

The properties calculation are performed in batch over thousands of structures. Task monitor is run with Linux Crontab service for periodically checking of job status and submission. This helps accelerate the computing process with some parallelism.

### 3.2 Density Clustering

An R CRAN package implementing the density based clustering algorithm by Alex Rodriguez and Alessandro Laio [29] is incorporated in this data pipeline. This package ‘densityClust’ provides robust tools to generate the initial  $\rho$  and  $\delta$  values for each observation as well as to use these thresholds to assign observations to clusters. Since this is done in two passes, it is free to reassign observations to clusters using a new set of  $\rho$  and  $\delta$  thresholds, without needing to recalculate everything.

### 3.3 Parallel Implementation of K-Means Algorithm

The parallel K-Means algorithm is implemented with OpenACC. OpenACC is a user-driven directive-based performance-portable parallel programming model designed to help scientists and engineers to porting their codes over a wide-variety of heterogeneous platform with significantly less programming effort than that with a low-level model (<https://www.OpenACC.org/>).

OpenACC takes use of the computing power of GPU and it is CUDA related. This programming model is therefore based on the heterogeneous architecture. The hardware model is shown in Fig. 4.

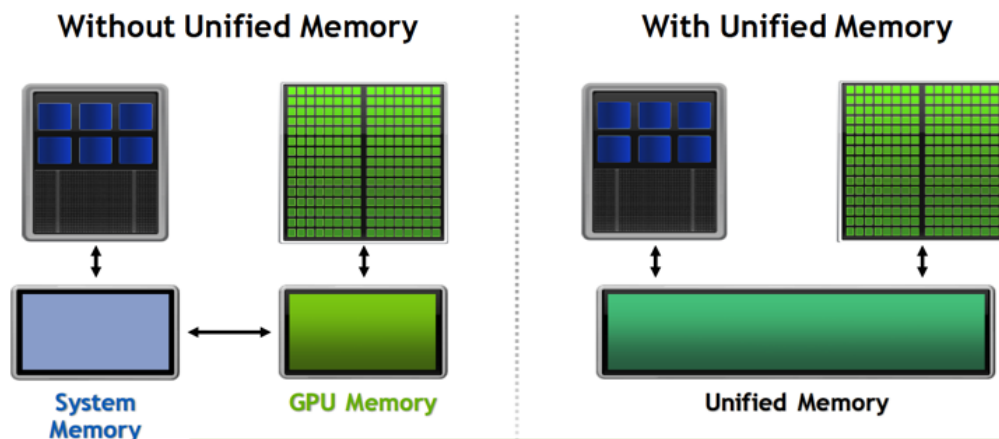


Figure 4: The heterogeneous architecture for OpenACC (<https://www.OpenACC.org/>).

Without unified memory, the data needs to be copied from CPU end to GPU end through PCIe. With this programming model, the K-means algorithm can be accelerated in following porting cycles.

### 3.3.1 3 Steps to Accelerate with OpenACC

Acceleration of a serial program can be divided into 3 steps **Analysis, Parallelization, Optimization**. The analysis focuses on the most time-consuming part of a serial program. Usually it is multiple loops over massive data. Parallelization adds on appropriate directives to highlight where the parallelism lies. Optimization usually focuses on the data movement between CPU and GPU end.

### 3.3.2 Parallel Directives

In previous section 2, we have already analyzed the parallelism in K-means Clustering algorithm. Therefore we should use the methods, the **kernels** and **parallel** directives, provided by OpenACC to parallelize the corresponding area.

**[kernels]** Using kernels simply leave the parallelism initialization to the compiler. One can use the kernels to automatically parse the region, and analyze potential parallelization capabilities. The kernels construct is very easy to use. Here is a simple example of using kernel directive.

```
9 #pragma acc kernels
10 {
11   for(i = 0; i < n; i++){
12     y[i] = 0;
13     x[i] = i+1;
14   }
15   for(i = 0; i < n; i++){
16     y[i] = 2 * x[i];
17   }
18 }
```

By looking at the compile information, we can tell that the parallelism is automatically initialized by the compiler. The line 9 shows the data transfer of matrix X and Y from host to device memory. The compiler automatically recognizes the parallelism in the “for” loop starting from line 11 and generates a parallel loop operation correspondingly. The gang in line 11 is a thread block and the thread in CUDA is called vector in OpenACC.

However, kernels directives does not guarantee the initialization of parallel loop. The compiler is poor at determining data dependency. It will not parallelize the loop that fails the dependency analysis. Then it will be developers’ responsibilities

to parallel.

```
1 9, Generating copyout(x[:],y[:])
2 11, Loop is parallelizable
3 Accelerator kernel generated
4 Generating Tesla code
5 11, #pragma acc loop gang, vector(32) /* blockIdx.x threadIdx.x */
6 15, Loop is parallelizable
7 Accelerator kernel generated
8 Generating Tesla code
9 15,#pragma acc loop gang, vector(32) /* blockIdx.x threadIdx.x */
```

**[parallel loop]** As mentioned above, using “parallel loop” transfers the responsibility to identify the parallelism to the developer. The “parallel” notifies the compiler to generate one or more parallel gangs, which execute redundantly and the “loop” directive informs the compiler which loop to parallelize. Sometimes the two directives can be used separately. Namely, the “loop” can be used singly before the loops which you believe have parallelism inside “parallel” region.

A big advantage to parallelize the loops of “parallel loop” over “kernels” is shown as follows. When the “kernels” fails to recognize parallel loop for potential pointer aliasing issue, the developer could still use the “parallel” and “loop” to parallelize it. When using “kernels”, we find the failure to recognize parallel loop according to the profiling information.

```
4 void setArrays(int *x, int *y, int n){
5     int i;
6     #pragma acc kernels
7     {
8         for(i = 0; i < n; i++){
9             y[i] = 0;
10            x[i] = i+1;
11        }
12        for(i = 0; i < n; i++){
13            y[i] = 2 * x[i];
14        }
15    }
16 }
```

The line 8 and 12 loops are not recognized as parallel loop by the compiler for potential pointer aliasing issue. The pointer aliasing refers to two arrays shares the same memory. The compiler can not determine it at compile time. Therefore the loops are kept for serial implementation for being safe.

```

1 6, Generating copyout(x[:n],y[:n])
2 8, Complex loop carried dependence of y-> prevents parallelization
3 Loop carried dependence of x-> prevents parallelization
4 Loop carried backward dependence of x-> prevents vectorization
5 Accelerator scalar kernel generated
6 Accelerator kernel generated
7 12, Complex loop carried dependence of x-> prevents parallelization
8 Loop carried dependence of y-> prevents parallelization
9 Loop carried backward dependence of y-> prevents vectorization
10 Accelerator scalar kernel generated
11 Accelerator kernel generated

```

If developer is sure about no pointer aliasing issue, developer can use “parallel loop” to enforce the parallelism to the compiler at this loop as follows.

```

4 void setArrays(int *x, int *y, int n){
5     int i;
6
7     #pragma acc parallel loop
8     for(i = 0; i < n; i++){
9         y[i] = 0;
10        x[i] = i+1;
11    }
12    #pragma acc parallel loop
13    for(i = 0; i < n; i++){
14        y[i] = 2 * x[i];
15    }
16 }

```

The loop at line 8 and 13 are therefore implemented parallel.

```

1 7, Accelerator kernel generated
2 Generating Tesla code
3 8, #pragma acc loop gang, vector(128) /* blockIdx.x threadIdx.x */
4 7, Generating copyout(x[:],y[:])
5 12, Accelerator kernel generated
6 Generating Tesla code
7 13, #pragma acc loop gang, vector(128) /* blockIdx.x threadIdx.x */
8 12, Generating copyout(y[:])
9 Generating copyin(x[:])

```

Besides, the pointer aliasing issue can be avoided with **restrict** keyword. With restrict before array y in declaration, “int \*restrict y”, the loops can also be recognized by compiler using “kernels”.

### 3.3.3 Optimization Techniques

Optimization of OpenACC techniques is a broad topic. Here we mainly discussed the data directives in OpenACC and how it could be used in K-means algorithm. Commonly used data directives are given as follows.

1. **copyin**: allocate memory on GPU and copies data from host to GPU when entering region.
2. **copyout**: allocate memory on GPU and copies data to the host when exiting region.
3. **copy**: allocate memory on GPU and copies data from host to GPU when entering region and copies data to the host when exiting region. (Structured Only)
4. **create**: allocate memory on GPU but not copy.
5. **delete**: deallocate memory on the GPU without copying. (Unstructured Only)
6. **present**: data is already present on GPU from another containing data region.

An obvious use of data directives in K-means algorithm is the **copyin** for source data. Since the data points will not be updated during the computation. Therefore, we could reduce the memory traffic without copying out the source data to the CPU end.

For more materials about OpenACC programming, please refer to OpenACC official recommendations at <https://www.OpenACC.org/resources>.

## 4 Results

### 4.1 Grain boundary energy as a function of angle and atomic density

Through the evolutionary search over a wide tile angle range ( $11.42^\circ \leq \theta \leq 79.61^\circ$ ), different GB structures are discovered. There are three popular types of GB structures in Fig. 5. These representative structures are different from each other in the structure unit called kite.

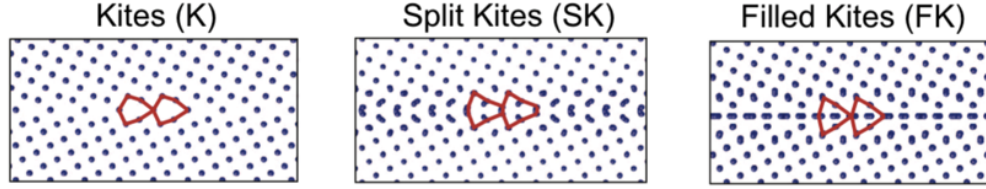


Figure 5: Representative structures from three popular kites family of GB structures [35].

Structures from three kites families also have their variations over a wide range of tilt angles. The mutations of split kites(SK) structure are shown in Fig. 6. Split Kites have higher atomic density compared to Kites as extra atoms occupy interstitial positions between [001] planes.

Another very important kite family in the high tilt angel range is Extended Kite. Extended Kites have higher atomic density compare to Kites, which correspond to half of the atomic plane in Fig 7. The structural units are outlined and change their separation with the increasing misorientation angle.

By varying misorientation angle and atomic density, the energy map of grain boundary phases can be derived easily. It is shown in Fig 8 that the Split Kite dominates the lower-angle grain boundary while most of grain boundary structures with higher tilt angles are Extended Kite. In the middle between high and low angle region, the Kite structure has lowest energy. The structures on convex hulls of Fig 8 are determined through eye detection for its small quantity.

## 4.2 Clustering results for the grain boundary

The evolutionary search is a very efficient methodology to discover grain boundary structures automatically. It usually will sample thousands of different grain boundary structures, which lead to the challenge in analyzing such a large amount of data. The Fig 9 shows the clustering results of around 1000 structures in the 2-dimensional space of excess stress and volume. The direction of the excess stress  $F_x$  is parallel to the tilt axis. It is clear to see that the excess stress and volume are effective order parameter pair to distinguish different kite structures. However, this clustering behavior is discovered through laboring and time-consuming eye-detection process. It is therefore necessary to improve this process with an intelligent algorithm to find good order parameters and to detect the clusters.

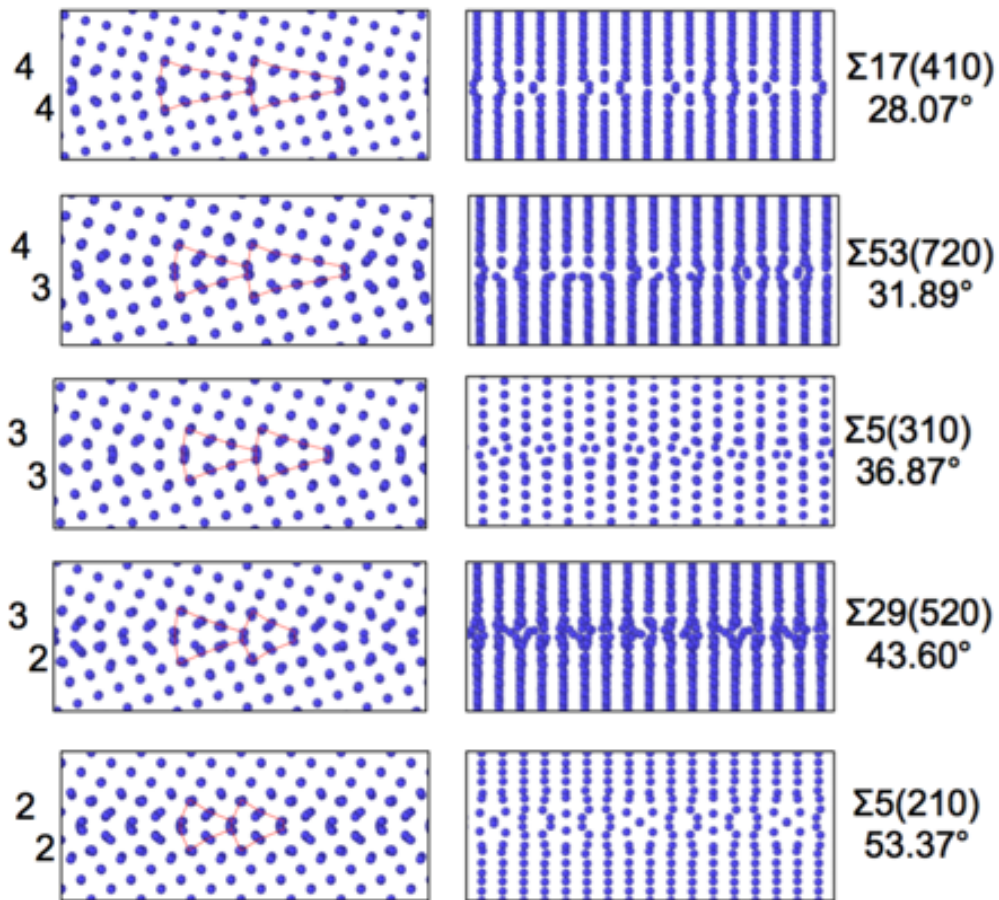


Figure 6: Split Kite Family. Split kites of five representative boundaries predicted by the evolutionary search and clustering analysis. These GB structures are viewed parallel to [001] tilt axis in left column and normal to it in right column.



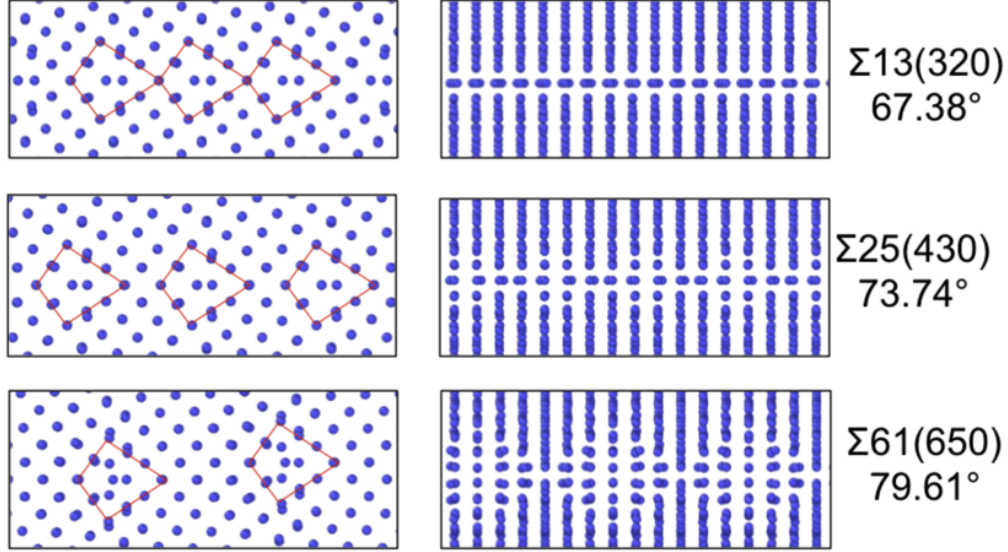


Figure 7: Extended Kite family. Three representative Extended Kite phases are predicted by the evolutionary search at 0 K. The misorientation angles are indicated on the figure. For each misorientation GB structures as viewed parallel to the [001] tilt axis in left and normal to it in right.

As described in Section 2.2.1, the density-based clustering algorithm is very promising to automate the analysis process. Its first step is to find good cluster centers in the decision graph which is composed of local density  $\rho$  and  $\delta$  the shortest distance to point with higher density. Seeing that the  $\rho$  and  $\delta$  of are all sensitive to the choice of criterion distance  $d_c$ , it is reasonable to vary  $d_c$  when plotting decision graph. A DC value which defines the neighbor rate between 1 and 2 percent are used as the minimal unit to vary the criterion distance.

The Fig 10 shows the decision graphs of  $\Sigma 5(210)$  when the criterion distance is set to be 1DC, 1.56DC and 2DC respectively. Only when 2DC is used to compute the  $\rho$  and  $\delta$ , we find reasonable cluster centroids with higher local density and longer distance to points of more neighbors. According to these decision graphs, 2DC is selected to evaluate the  $\delta$  and  $\rho$  of every data point. The group is thereafter assigned for each point.

The clustering behavior of  $\Sigma 5(210)$  system can be further explored by visualizing these groups of points on different 2D feature maps. By looking the clustering performance of various feature pairs, we could decide good order parameters to

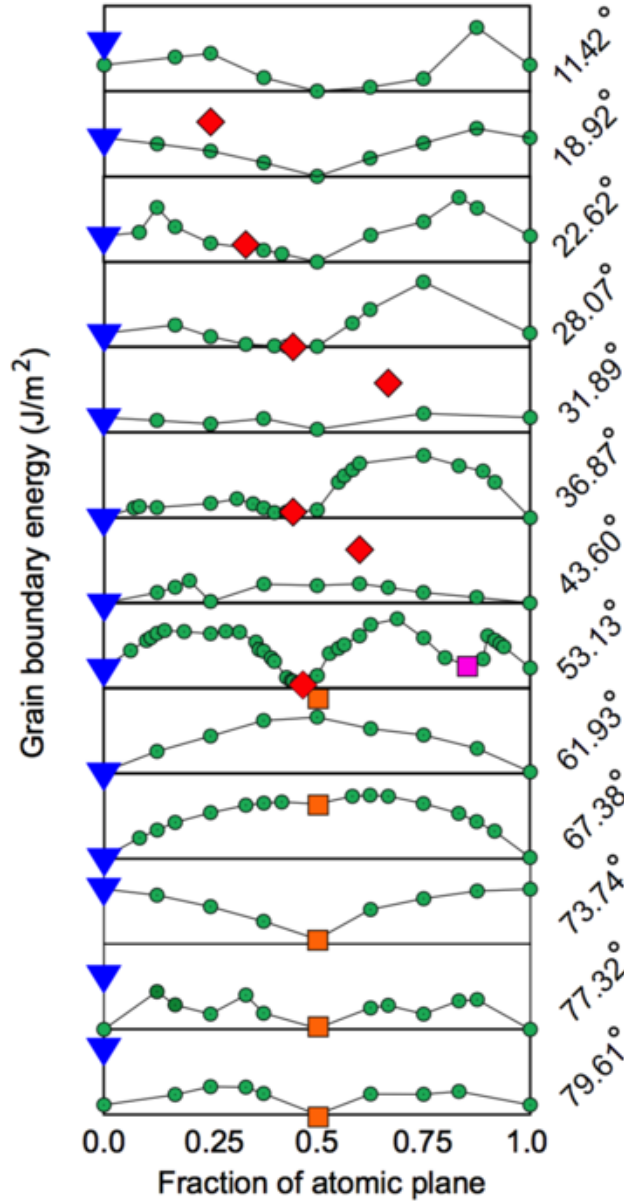


Figure 8: Evolutionary search and clustering identify new ground states and multiple grain boundary phases. The search explores different atomic densities and finds low-energy grain boundary configurations (green circles) ignored by the conventional methodology. With same tilt angle  $\theta$  atomic fractions and energies of each grain boundary at 0 K are colored by blue triangles for Kite family, red diamonds for Split Kite family and orange squares for Extended Kite family.

distinguish different GB structures.

We defined the GB structures in a 8-dimensional feature space. There are 28 different ways to map these structures into 2-dimensional subspaces. For most

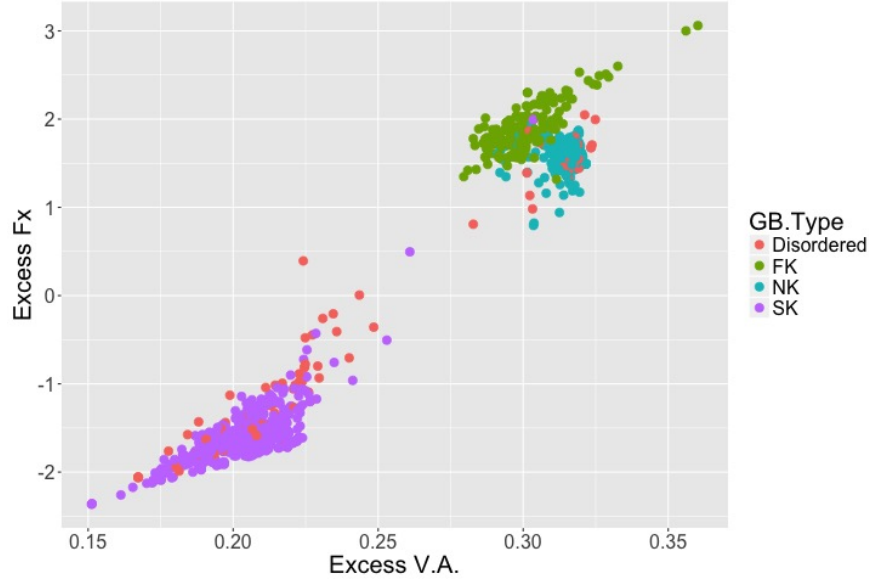


Figure 9: Eye detection of  $\Sigma 5(210)$  in the 2-dimensional space of excess stress and volume, where the direction of excess stress  $F_x$  is parallel to tilt axis. The orange dots correspond to distorted structures while the green, blue and purple are for Filled Kite(FK), Normal Kite(K or NK) and Split Kite(SK) respectively.

of feature pairs, we see very impressive clustering results for  $\Sigma 5(210)$  system. Some of them are listed in Fig 11. Comparing Fig 11(c) and Fig 9, it is clear to see that the density based algorithm yields very successful clustering results, which is as good as eye detection. In  $\Sigma 29(520)$  system, we also see these encouraging results. What these results imply is that these feature are promising order parameters to cluster system with clustering behavior. This could greatly reduce the work load to analyze and define every structure manually. Most of the high angle GB structures show this intense clustering behaviors while for many lower tilt-angle system, very few feature pairs are effective to distinguish different GB structures. The latter point will be discussed in detail in the following section.

### 4.3 Clustering of Grain Boundaries with Low Tilt Angle

The  $\Sigma 29(520)$  system has close tilt angle to  $\Sigma 5(210)$  system. The tilt angles are  $53.13^\circ$  and  $43.60^\circ$  respectively for  $\Sigma 29(520)$  and  $\Sigma 5(210)$  system. We also observe satisfactory but not perfect clustering results in  $\Sigma 29(520)$  system as shown in Fig 12. However, the performance of excess energy and atomic fraction pair is not as ideal as that in  $\Sigma 5(210)$  system.

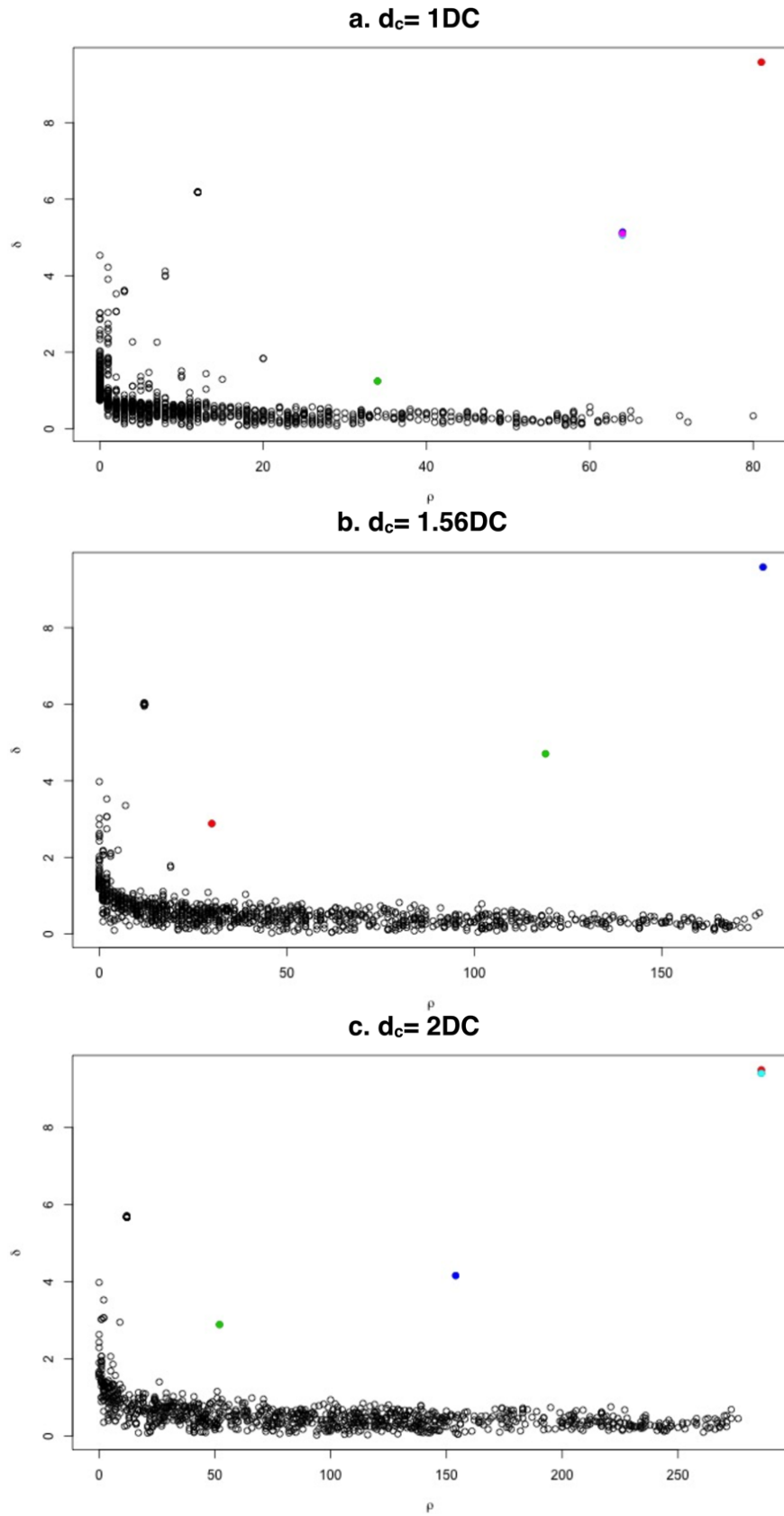


Figure 10: Decision graph of  $\sum 5(210)$  when the criterion distance is equal to (a)1DC, (b)1.56DC, (c)2DC.

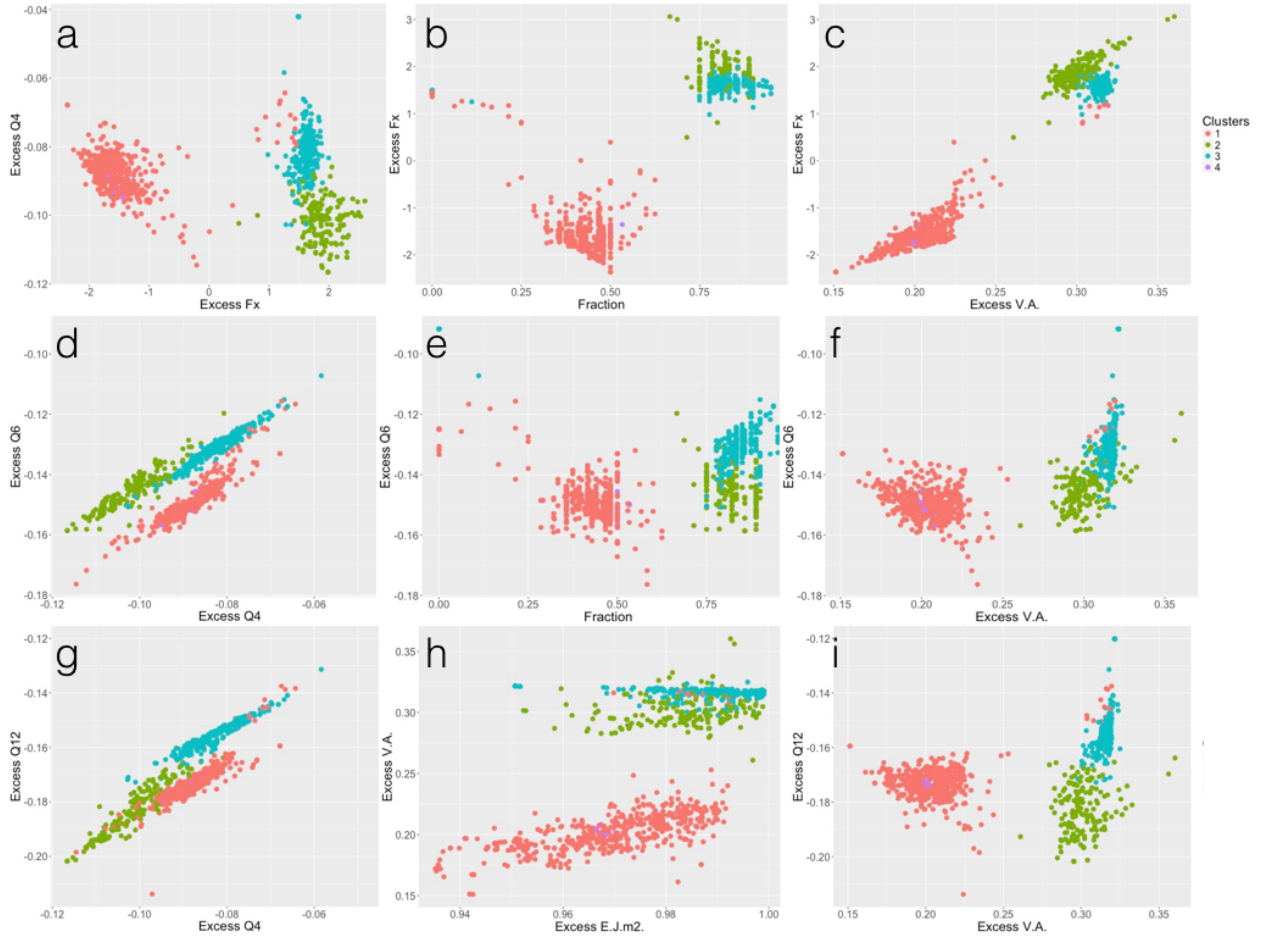


Figure 11: The clustering of GB structures in  $\Sigma 5(210)$  system on different feature maps (a) Excess  $Q_4$  vs Excess Stress  $F_X$ , (b) Excess Stress  $F_X$  vs Atomic Fraction, (c) Excess Stress  $F_X$  vs Excess volume, (d) Excess  $Q_6$  vs Excess  $Q_4$ , (e) Excess  $Q_6$  vs Atomic Fraction, (f) Excess  $Q_6$  vs Excess Volume, (g) Excess  $Q_{12}$  vs Excess  $Q_4$ , (h) Excess Volume vs Excess Energy, (i) Excess  $Q_{12}$  vs Excess Volume.

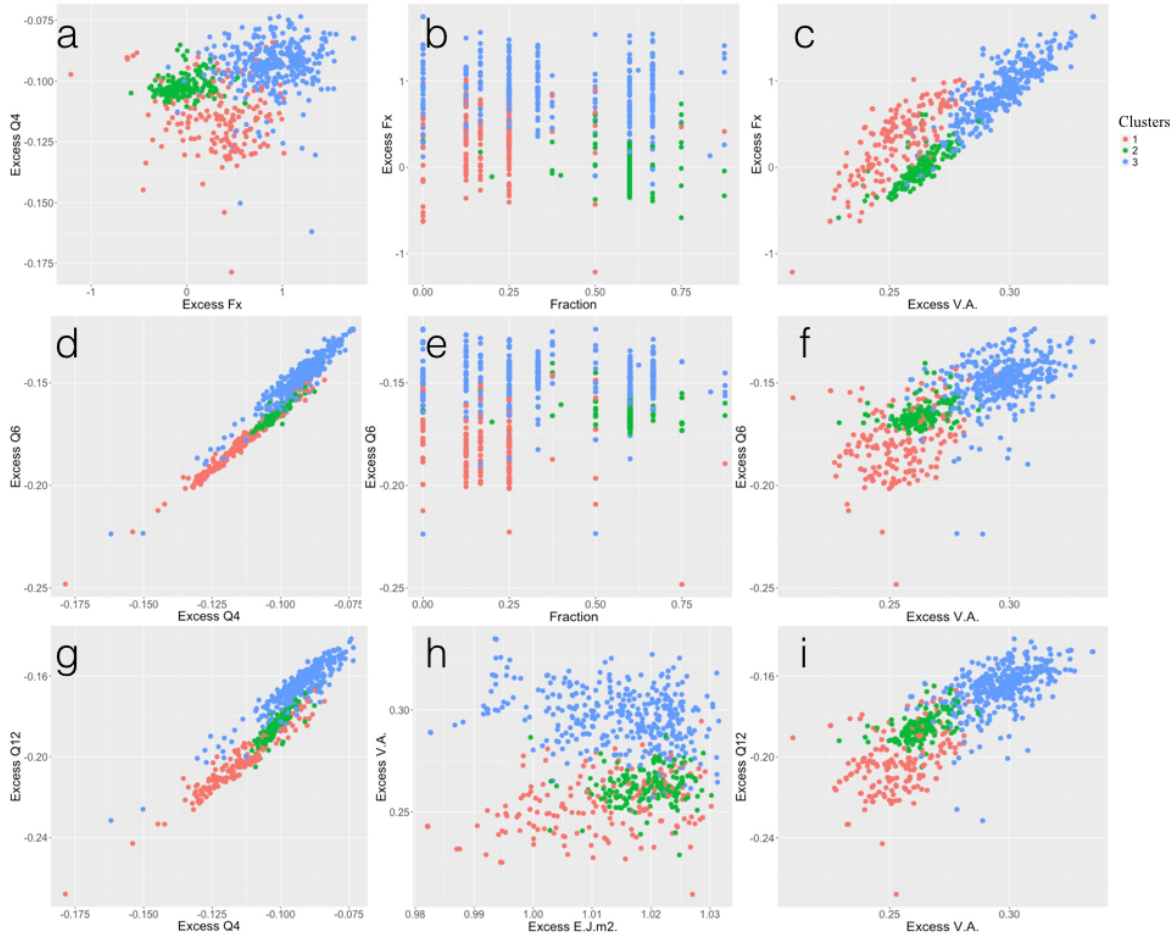


Figure 12: The clustering of GB structures in  $\Sigma 29(520)$  system on different feature maps (a) Excess  $Q_4$  vs Excess Stress  $F_X$ , (b) Excess Stress  $F_X$  vs Atomic Fraction, (c) Excess Stress  $F_X$  vs Excess volume, (d) Excess  $Q_6$  vs Excess  $Q_4$ , (e) Excess  $Q_6$  vs Atomic Fraction, (f) Excess  $Q_6$  vs Excess Volume, (g) Excess  $Q_{12}$  vs Excess  $Q_4$ , (h) Excess Volume vs Excess Energy, (i) Excess  $Q_{12}$  vs Excess Volume.

As mentioned in previous section, most feature pairs are no longer good order parameters for lower angle system like  $\Sigma 5(310)(\theta=36.87^\circ)$ ,  $\Sigma 17(410)(\theta=28.07^\circ)$  and *etc.*. Usually the clustering are not satisfactory for the system with tilt angle under  $36.87^\circ$ . The failure of these feature pairs comes from the disordered structures or transitory structures existing in these low tilt angle system.

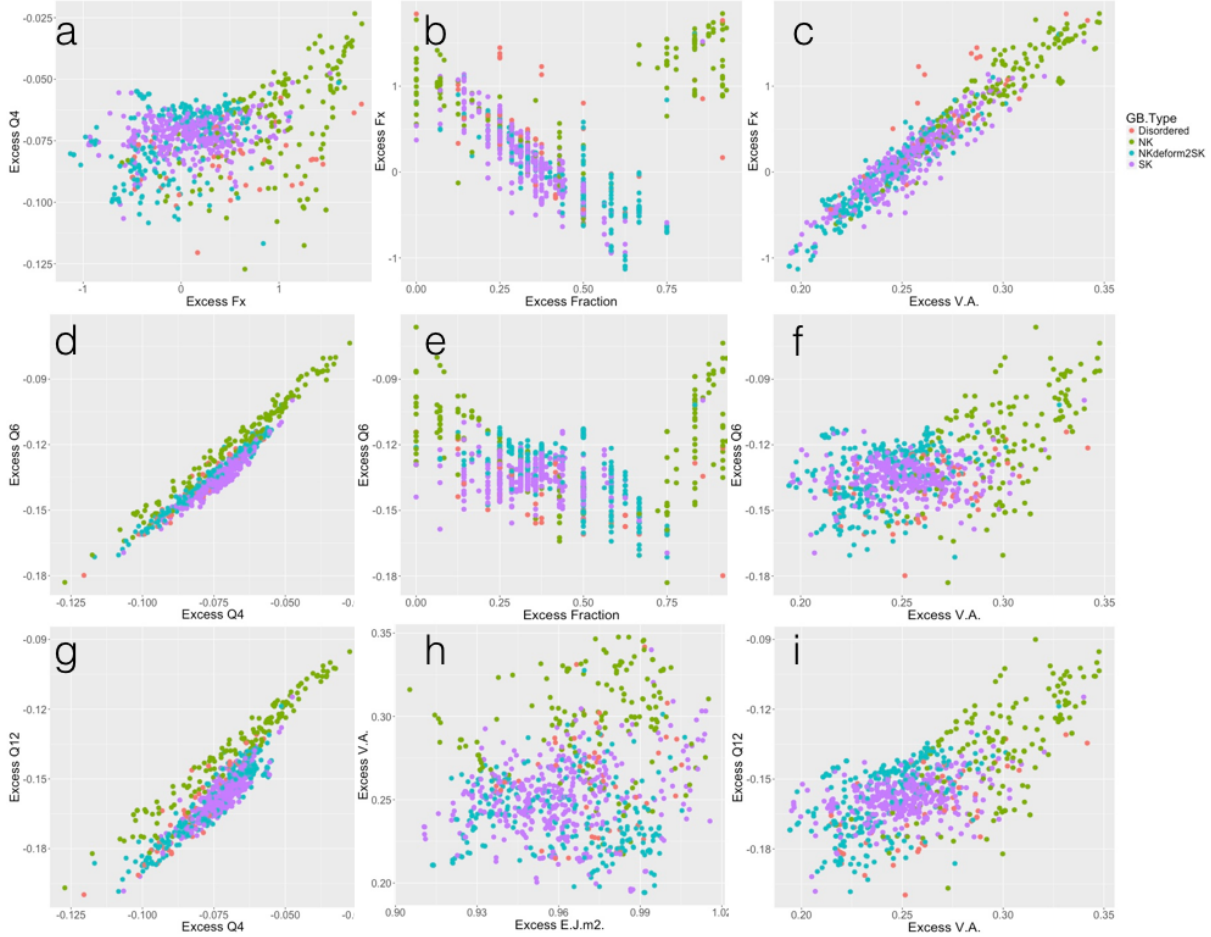


Figure 13: The clustering of GB structures in  $\Sigma 5(310)$  system on different feature maps (a) Excess  $Q_4$  vs Excess Stress  $F_X$ , (b) Excess Stress  $F_X$  vs Atomic Fraction, (c) Excess Stress  $F_X$  vs Excess volume, (d) Excess  $Q_6$  vs Excess  $Q_4$ , (e) Excess  $Q_6$  vs Atomic Fraction, (f) Excess  $Q_6$  vs Excess Volume, (g) Excess  $Q_{12}$  vs Excess  $Q_4$ , (h) Excess Volume vs Excess Energy, (i) Excess  $Q_{12}$  vs Excess Volume.

In Fig 13, we mapped the structures determined by eyes detection on 2-dimensional feature space. The clustering behavior is much less clear than that in  $\Sigma 5(210)$  system. Only  $Q_6$  and  $Q_4$  well classified all of three GB structures, while the structure labeled as ‘NKdeform2SK’ overlaps with Split Kite (SK) structure. The ‘NKdeform2SK’ structure is actually a transitory structure between Kite family (NK) and Split Kite family (SK) according to Fig 14 since its structure unit can be regarded

as either deformed SK unit or deformed NK unit. According to overlapping between SK and NKdeform2SK structure in Fig 13, the NKdeform2SK structure is closer to SK structure in the feature space, which implies their similarities in structural and energetic properties.

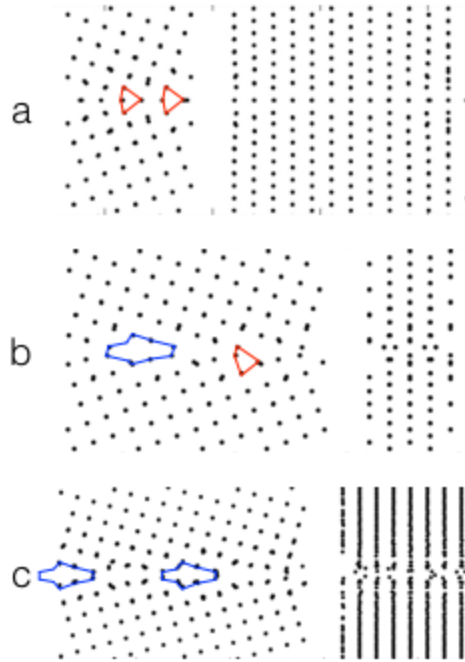


Figure 14: The GB structures in  $\sum 5(310)$  system (a) Kite Family (NK or K), (b) NKdeform2SK , (c) Split Kite family (SK).

For system with lower tilt angle like  $\sum 37(610)$  ( $\theta=18.92^\circ$ ) and  $\sum 25(710)$  ( $\theta=16.26^\circ$ ), the structures are even more complex. The complexity rises from the existence of mixed Kite and Split Kite structures and the transitory structures between these two kite families. These structures are usually disordered or partially ordered compare two kite families. In feature space, they usually overlaps with the two kite families for their partial structural similarities. These overlapping leads to the failure of clustering in current feature space. Therefore we hardly see clear clustering results when mapping them onto planes composed by any feature pairs. The Steinhardt Order Parameters, which is effective for  $\sum 5(310)$ , fail in the system of  $\sum 37(610)$  as shown in Fig 16 since the disordered and transitory structures like ‘NKdeform2SK’, ‘NKmixSK’, ‘NKBigKitedeform2SK’ in Fig overlaps with NK and SK and blur the boundary between the two kite families.



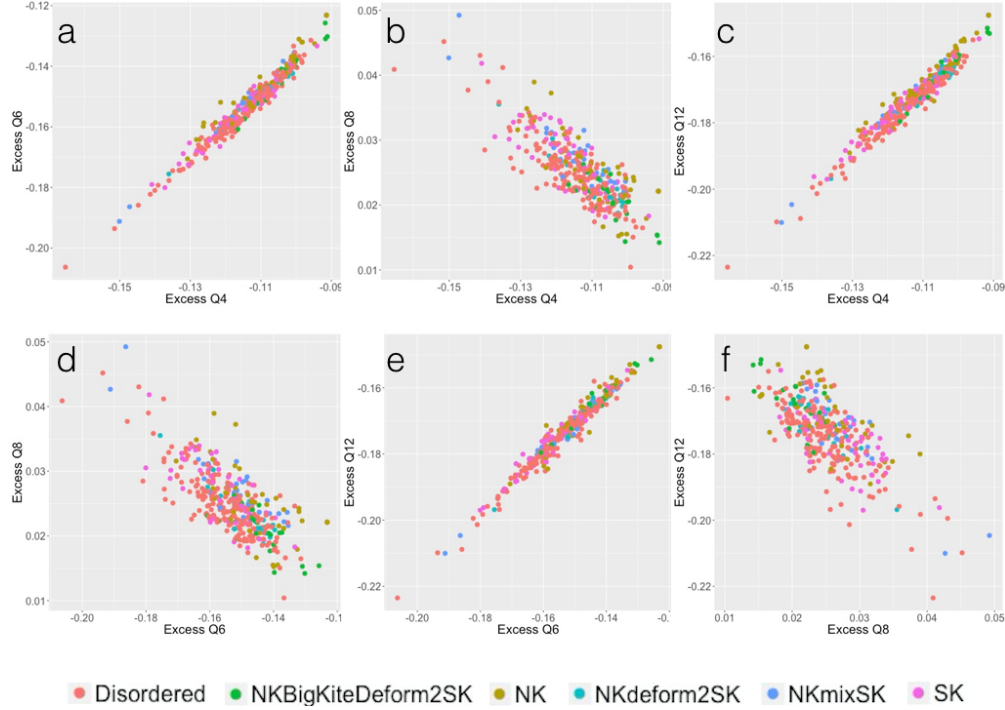


Figure 15: The GB structures in  $\sum 5(310)$  system (a) Kite Family (NK or K), (b) NKdeform2SK , (c) Split Kite family (SK).

## 5 Discussions

The development of this data pipeline helps understand the grain boundary structures and properties. Atomic arrangements in Cartesian coordinate system pose challenges to directly categorize a large number of structures. The feature engineering part of this data pipeline performs dimension reduction for each structures by mapping each structure into a space of 8 dimensions. Furthermore, the clustering analysis part of this data pipeline group these structures according to their distribution in the new space. A density based clustering algorithm [29] is used here to efficiently to find the group centroids and assign each structures.

The results are very intriguing and insightful. Structures are clustered into different groups very well and structures in different groups show different structure units at grain boundary region. These structures units are generalized as Kite, Split Kite, Filled and Extended Kite families respectively. However, when the tilt angle gets smaller, which means the grain boundary region is more compressed, more and more mixed and disordered kite families dominate the grain bound-

ary structures. Some of them are the mixture of Normal Kite and Split Kite or intermediates of these two families. Generally, grain boundary structures have more diversity in lower tilt angle system while structures become more ordered in higher tilt angle system.

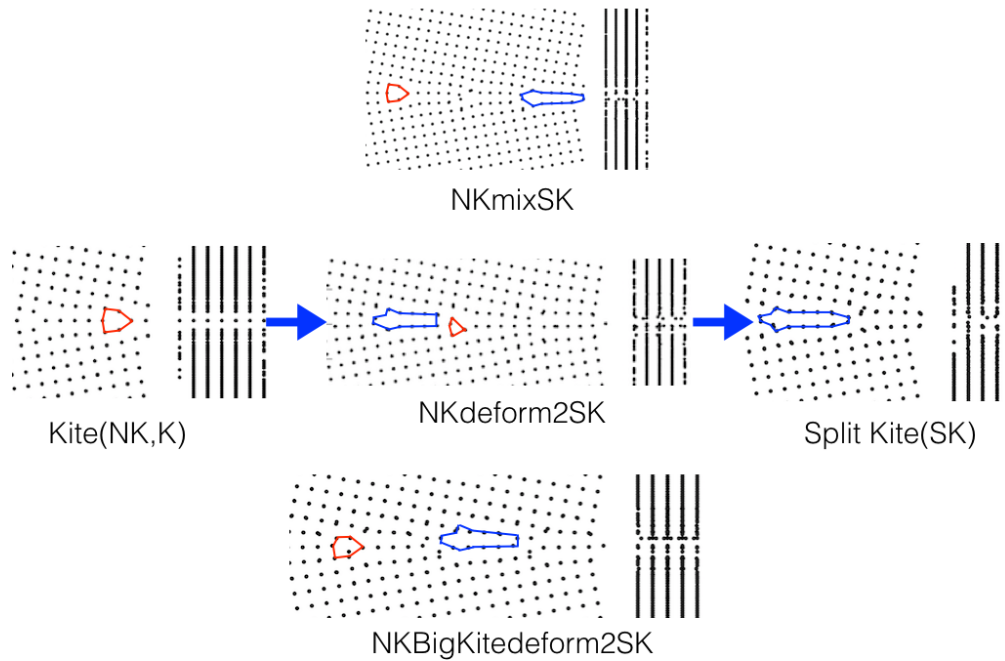


Figure 16: The GB structures in  $\Sigma 37(610)$  system Kite Family (NK or K) in the left , NKmixSK, NKdeform2SK and NKBigKitedeform2SK in the middle while Split Kite family (SK) in the right.

The current clustering is performed over structures at ambient pressure and 0 K and yields several different grain boundary families. It will be very interested to investigate grain boundary structures under different temperatures, which will reveal the phase diagram information of Grain Boundaries. It will also be a very fascinating topic to research on the evolution between different grain boundary structures with newly developed method like Transition Path Sampling method [36]. My recent work imply the potential to adapt this method to investigate the bulk phase transition [37].

The parallel K-means algorithm function is implemented here and left for future big data application. For this grain boundary problem, the density based

clustering algorithm already yields very satisfying results efficiently.

## 6 Acknowledgments

The work was funded by the Laboratory Directed Research and Development Program at Lawrence Livermore National Laboratory(LLNL) under project tracking code 17-LW-012. Prof. Qiang Zhu at University of Las Vegas, Nevada predicted grain boundary structures with evolutionary algorithm. Dr. Timofey Frolov at LLNL provided helpful suggestions on the feature properties calculations to grain boundary structures. Prof. Norman S. Matloff at University of California, Davis advised me during this project.

## 7 Running Demo

The running of the data pipeline is given to Cu  $\Sigma$ 29(520) as a demo.

Enter the computation directory.

```
1 ***** Step 1. Run the Properties Calculation *****
2 ***** 1.1 Run the Calculation *****
3 >> cd Cu520
```

Rescale the dimension and atoms coordinates of predicted structures to be consistent with correct lattice parameter 3.615 for Cu face center cubic cell of 4 atoms with  $a=b=c$  and  $\alpha=\beta=\gamma=90^\circ$ . The **LAMMPS\_backup** is the input structure directory and the **LAMMPS\_backup\_new** is the rescaled structure output directory.

```
1 >> nohup ./convert.py LAMMPS.backup LAMMPS_backup_new 3.615 5 2 0 &
```

Perform the properties calculation over the rescaled structures, you can track the calculation progress from **progress** file in current directory while all the structures's properties are collected in **STRUCTURES.dat** file. Here the potential file **Cu01.eam.alloy.txt** is assigned for atomic interactions used in LAMMPS structure local optimization.

**NOTE:** During this calculation, you can check the 'progress' file to track the progress.

```
1 >> nohup ./pipe.py LAMMPS_backup_new Cu01.eam.alloy.txt 5 2 0 fcc Cu &
```

```
1 ***** 1.2 SUMMARY of Results *****
2 **** 1.2.1 about the calc folder ****
```

After finishing the above calculation, there will be 10 calculation folder, **calc1**, **calc2**, **calc3**, ..., **calc10**. For structure LAMMPS.#X, it will be computed under calc#T, where  $T = X \% 10$  if  $X \% 10 \neq 0$  and  $T = 10$  if  $X \% 10 == 0$ . For example, LAMMPS\_0001 is calculated in calc1 folder and LAMMPS\_0010 is calculated in **calc10** folder. In each calculation folder, you will find the following calculation files. Let us look into the calculation to structure indexed by 579 under **calc9**.

```

1 >> ls -al ./calc9/*0579*
2 -rw-r--r--@ 1 BingxiLi  staff      759 Dec  5 17:19 ./calc9/SUBMIT_lammps_0579
3 -rw-r--r--@ 1 BingxiLi  staff       84 Dec  5 17:19 ./calc9/lammps_0579.error
4 -rw-r--r--@ 1 BingxiLi  staff    6005 Dec  5 17:19 ./calc9/lammps_0579.in
5 -rw-r--r--@ 1 BingxiLi  staff    7810 Dec  5 17:19 ./calc9/lammps_0579.output
6 -rw-r--r--@ 1 BingxiLi  staff  324351 Dec  5 17:19 ./calc9/lammps_0579.struc
7 -rw-r--r--@ 1 BingxiLi  staff   36772 Dec  5 17:19 ./calc9/lammps_0579_low.
   struc
8 -rw-r--r--@ 1 BingxiLi  staff   36624 Dec  5 17:19 ./calc9/lammps_0579_up.
   struc

```

Here is the explanation:

1. SUBMIT\_lammps\_0579: show how to SUBMIT the calculation. If you want to repeat the calculation, please run 'sbatch ./calc9/SUBMIT\_lammps\_0579'.
2. lammps\_0579.in: the lammps input for the properties calculation to structure 0579.
3. lammps\_0579.error and lammps\_0579.output: lammps output files.
4. \*.Struc: lammps dump file generated at the end of lammps calculation. It contains x, y, z coordinates and different properties for each atoms in the gb structure. More in details:
  - (a) lammps\_0579.struc: the coordinates and properties information for all the atoms in the structures
  - (b) lammps\_0579\_low.struc: the coordinates and properties information for atoms in the selected bulk region in lower layer.
  - (c) lammps\_0579\_up.struc: the coordinates and properties information for atoms in the selected bulk region in upper layer.

**NOTE:** The bulk region in lower and upper layer here use the region that is 10A far from their surface. This choice are validated effective in Step 2.

The **STRUCTURES.dat** listed the excess properties for each structures. Here is an example of its content.

```

1 **** 1.2.2 about the STRUCTURES.dat ****
2 >> head -2 STRUCTURES.dat
3   Structures      Fraction  E[J/m2]    V[A]       Fx         Fy         Fz
4   Q4              Q6        Q8         Q12
   lammps_0001    0.00000  0.98299   0.28863   1.37559   0.51736   -0.00640
   -0.09975     -0.14718  0.01992   -0.16804

```

The following shows how to verify the properties results by comparing the neighborhood of grain boundary region to ideal bulk. When neighborhoods have close value to ideal bulk which means the structure is well relaxed.

```

1 ***** Step 2. Validate the Results *****
2 ***** 2.1 Run the Calculation *****

```

Generates **AVGSTDS\_lowbulk.dat** and **AVGSTDS\_upbulk.dat** to store two side neighborhood regions' property results. Plot over **AVGSTDS\_lowbulk.dat** and **AVGSTDS\_upbulk.dat** and figures will be saved to **AVGSTDS\_lowbulk\_plots** and **AVGSTDS\_upbulk\_plots** respectively.

```

1 >> ./avgstd_lowbulk.py LAMMPS.backup_new/
2 >> ./avgstd_upbulk.py LAMMPS.backup_new/
3 >> ./avgstd_bulkplots.py AVGSTDS_lowbulk.dat AVGSTDS_lowbulk_plots
   AVGSTDS_upbulk.dat AVGSTDS_upbulk_plots

```

Sometimes there will be great discrepancy between neighborhood bulk and ideal bulk, which means the grain boundary is either poorly relaxed or falsely assigned. Usually the latter reason is more likely since the previous calculation assign the grain boundary region artificially. Namely, we simply set it as a fixed region within a certain distance range in previous run. In the case where discrepancies arise, we need to rerun the properties with following commands. By doing this, we could dynamically assign accurate grain boundary according to energy and Steinhardt Order Parameters. The **rerun.py** generates **STRUCTURESnew.dat** to store properties of newly assigned grain boundary regions and **AVGSTDS\_lowbulknew.dat**, **AVGSTDS\_upbulknew.dat** to store properties for new neighborhoods. By plotting and comparing, we could see the robustness of this way to finding accurate grain boundary regions.

```

1 >> nohup ./rerun.py ./LAMMPS.backup_new/ 5 2 0 &
2 >> ./avgstd_bulkplots.py AVGSTDS_lowbulknew.dat AVGSTDS_lowbulk_plots_new
   AVGSTDS_upbulknew.dat AVGSTDS_upbulk_plots_new

```

The following shows simple clustering analysis operations.

```
1 ***** Step 3. Analyze the Results *****  
2 $ Rscript DClust.R ../STRUCTURESnew.dat 1.56 20 2
```

The script **DClust.R** takes 4 arguments. The first one **STRUCTURESnew.dat** is the properties file and the second one sets how many times of default distance criterion, which is selected to make neighbor rates between 1%–2%. The third and fourth one assign the  $\rho$  and  $\delta$  criterion to select centroids on decision graph. Clustering results visualized on different 2-D plots will be output to **DClustAnalysis\_plots/** directory and the corresponding decision graph can also be found as **Decision Graph** in that directory.

## References

- [1] Shen J Dillon, Ming Tang, W Craig Carter, and Martin P Harmer. Complexion: A new concept for kinetic engineering in materials science. *Acta Materialia*, 55(18):6208–6218, 2007.
- [2] Patrick R. Cantwell, Ming Tang, Shen J. Dillon, Jian Luo, Gregory S. Rohrer, and Martin P. Harmer. Grain boundary complexions. *Acta Materialia*, 62:1 – 48, 2014.
- [3] J.M. Rickman, H.M. Chan, M.P. Harmer, and J. Luo. Grain-boundary layering transitions in a model bicrystal. *Surface Science*, 618:88 – 93, 2013.
- [4] Ming Tang, W Craig Carter, and Rowland M Cannon. Grain boundary transitions in binary alloys. *Physical review letters*, 97(7):075502, 2006.
- [5] Ming Tang, W Craig Carter, and Rowland M Cannon. Diffuse interface model for structural transitions of grain boundaries. *Physical Review B*, 73(2):024102, 2006.
- [6] Jian Luo, Haifeng Wang, and Yet-Ming Chiang. Origin of solid-state activated sintering in  $\text{Bi}_2\text{O}_3$ -doped  $\text{ZnO}$ . *Journal of the American Ceramic Society*, 82(4):916–920, 1999.
- [7] Jian Luo, Huikai Cheng, Kaveh Meshinchi Asl, Christopher J Kiely, and Martin P Harmer. The role of a bilayer interfacial phase on liquid metal embrittlement. *Science*, 333(6050):1730–1733, 2011.
- [8] Wayne D Kaplan. The mechanism of crystal deformation. *Science*, 349(6252):1059–1060, 2015.
- [9] Margarita Kuzmina, Michael Herbig, Dirk Ponge, Stefanie Sandlöbes, and Dierk Raabe. Linear complexions: Confined chemical and structural states at dislocations. *Science*, 349(6252):1080–1083, 2015.
- [10] Mor Baram, Dominique Chatain, and Wayne D Kaplan. Nanometer-thick equilibrium films: the interface between thermodynamics and atomistics. *Science*, 332(6026):206–209, 2011.
- [11] Wolfgang Rheinheimer and Michael J Hoffmann. Non-arrhenius behavior of grain growth in strontium titanate: new evidence for a structural transition of grain boundaries. *Scripta Materialia*, 101:68–71, 2015.
- [12] Shen J Dillon, Kaiping Tai, and Song Chen. The importance of grain boundary complexions in affecting physical properties of polycrystals. *Current Opinion in Solid State and Materials Science*, 20(5):324–335, 2016.

- [13] Gregory S Rohrer. The role of grain boundary energy in grain boundary complexion transitions. *Current Opinion in Solid State and Materials Science*, 20(5):231–239, 2016.
- [14] KL Merkle and David J Smith. Atomic structure of symmetric tilt grain boundaries in nio. *Physical Review Letters*, 59(25):2887, 1987.
- [15] Chan Woo Park, Duk Yong Yoon, John E Blendell, and Carol A Handwerker. Singular grain boundaries in alumina and their roughening transition. *Journal of the American Ceramic Society*, 86(4):603–11, 2003.
- [16] Timofey Frolov, Mark Asta, and Yuri Mishin. Segregation-induced phase transformations in grain boundaries. *Physical Review B*, 92(2):020103, 2015.
- [17] T Frolov, M Asta, and Y Mishin. Phase transformations at interfaces: Observations from atomistic modeling. *Current Opinion in Solid State and Materials Science*, 20(5):308–315, 2016.
- [18] Artem R Oganov and Colin W Glass. Crystal structure prediction using ab initio evolutionary techniques: Principles and applications. *The Journal of chemical physics*, 124(24):244704, 2006.
- [19] Xiang-Feng Zhou, Xiao Dong, Artem R Oganov, Qiang Zhu, Yongjun Tian, and Hui-Tian Wang. Semimetallic two-dimensional boron allotrope with massless dirac fermions. *Physical Review Letters*, 112(8):085502, 2014.
- [20] Qiang Zhu, Li Li, Artem R Oganov, and Philip B Allen. Evolutionary method for predicting surface reconstructions with variable stoichiometry. *Physical Review B*, 87(19):195317, 2013.
- [21] Qiang Zhu, Vinit Sharma, Artem R Oganov, and Ramamurthy Ramprasad. Predicting polymeric crystal structures by evolutionary algorithms. *The Journal of chemical physics*, 141(15):154102, 2014.
- [22] Andriy O Lyakhov, Artem R Oganov, Harold T Stokes, and Qiang Zhu. New developments in evolutionary structure prediction algorithm uspx. *Computer Physics Communications*, 184(4):1172–1182, 2013.
- [23] S Von Alfthan, PD Haynes, K Kaski, and AP Sutton. Are the structures of twist grain boundaries in silicon ordered at 0 k? *Physical review letters*, 96(5):055505, 2006.
- [24] Alvin Ls Chua, Nicole A Benedek, Lin Chen, Mike W Finnis, and Adrian P Sutton. A genetic algorithm for predicting the structures of interfaces in multicomponent systems. *Nature materials*, 9(5):418, 2010.



- [25] Jian Zhang, Cai-Zhuang Wang, and Kai-Ming Ho. Finding the low-energy structures of si [001] symmetric tilted grain boundaries with a genetic algorithm. *Physical Review B*, 80(17):174102, 2009.
- [26] Paul J Steinhardt, David R Nelson, and Marco Ronchetti. Bond-orientational order in liquids and glasses. *Physical Review B*, 28(2):784, 1983.
- [27] T Frolov and Y Mishin. Thermodynamics of coherent interfaces under mechanical stresses. i. theory. *Physical Review B*, 85(22):224106, 2012.
- [28] Steve Plimpton. Fast parallel algorithms for short-range molecular dynamics. *Journal of computational physics*, 117(1):1–19, 1995.
- [29] Alex Rodriguez and Alessandro Laio. Clustering by fast search and find of density peaks. *Science*, 344(6191):1492–1496, 2014.
- [30] Lucien Le Cam, Jerzy Neyman, and Elizabeth L Scott. *Proceedings of the Sixth Berkeley Symposium on Mathematical Statistics and Probability: Held at the Statistical Laboratory, University of California, June 21-July 18, 1970*, volume 2. Univ of California Press, 1972.
- [31] Geoffrey J McLachlan and Thriyambakam Krishnan. Wiley series in probability and statistics. *The EM Algorithm and Extensions, Second Edition*, pages 361–369, 1997.
- [32] Mary Inaba, Naoki Katoh, and Hiroshi Imai. Applications of weighted voronoi diagrams and randomization to variance-based k-clustering. In *Proceedings of the tenth annual symposium on Computational geometry*, pages 332–339. ACM, 1994.
- [33] D Manning Christopher, Raghavan Prabhakar, and SCHÜTZE Hinrich. Introduction to information retrieval. *An Introduction To Information Retrieval*, 151:177, 2008.
- [34] David Arthur and Sergei Vassilvitskii. How slow is the k-means method? In *Proceedings of the twenty-second annual symposium on Computational geometry*, pages 144–153. ACM, 2006.
- [35] Qiang Zhu, Amit Samanta, Bingxi Li, Robert E. Rudd, and Timofey Frolov. Predicting phase behavior of grain boundaries with evolutionary search and machine learning. *submitted*, 2017.
- [36] Peter G Bolhuis, David Chandler, Christoph Dellago, and Phillip L Geissler. *Ann. Rev. Phys. Chem.*, 53(1):291–318, 2002.
- [37] Bingxi Li, Guangrui Qian, Artem R. Oganov, Salah Eddine Boulfelfel, and Roland Faller. Mechanism of the fcc-to-hcp phase transformation in solid ar. *The Journal of Chemical Physics*, 146(21):214502, 2017.